Available online at www.sciencedirect.com
ScienceDirect
Chemical Physics 341 (2007) 143–157
Chemical Physics
www.elsevier.com/locate/chemphys

Are water simulation models consistent with steady-state and ultrafast vibrational spectroscopy experiments?

J.R. Schmidt [a], S.T. Roberts [b], J.J. Loparo [b], A. Tokmakoff [b], M.D. Fayer [c], J.L. Skinner [a,*]

[a] Theoretical Chemistry Institute and Department of Chemistry, University of Wisconsin, Madison, WI 53706, United States
[b] Department of Chemistry, Massachusetts Institute of Technology, Cambridge, MA 02139, United States
[c] Department of Chemistry, Stanford University, Stanford, CA 94305, United States

Received 1 February 2007; accepted 18 June 2007
Available online 6 July 2007

Abstract

Vibrational spectroscopy can provide important information about structure and dynamics in liquids. In the case of liquid water, this is particularly true for isotopically dilute HOD/D_2O and HOD/H_2O systems. Infrared and Raman line shapes for these systems were measured some time ago. Very recently, ultrafast three-pulse vibrational echo experiments have been performed on these systems, which provide new, exciting, and important dynamical benchmarks for liquid water. There has been tremendous theoretical effort expended on the development of classical simulation models for liquid water. These models have been parameterized from experimental structural and thermodynamic measurements. The goal of this paper is to determine if representative simulation models are consistent with steady-state, and especially with these new ultrafast, experiments. Such a comparison provides information about the accuracy of the dynamics of these simulation models. We perform this comparison using theoretical methods developed in previous papers, and calculate the experimental observables directly, without making the Condon and cumulant approximations, and taking into account molecular rotation, vibrational relaxation, and finite excitation pulses. On the whole, the simulation models do remarkably well; perhaps the best overall agreement with experiment comes from the SPC/E model.

Keywords: Water; Vibrational spectroscopy; Dynamics; Simulation models

1. Introduction

The properties of water are of profound importance in many branches of science, from geology to biology to oceanography [1]. Water is particularly ubiquitous in chemistry, where it serves as a common solvent for many reactions. The polar nature of water indicates that it strongly solvates many types of charged or polar reactants, products, or intermediates, thus allowing chemists to carry out reactions that would not be possible in the gas phase, or in a non-polar solvent. Consider, for example, the prototypical nucleophilic substitution reaction of organic chemistry. In the non-concerted form of this reaction, involving a charged carbo-cation intermediate, a highly polar solvent such as water can speed the reaction by many orders of magnitude relative to non-polar solvents, by solvating and stabilizing the cationic intermediate [2]. Water also plays an essential role as solvent in almost all biologically relevant reactions and processes [3].

Given the vital role of water as an experimental solvent, it is not surprising that water plays in equally important role in molecular dynamics (MD) simulation. This is evidenced by the vast numbers of models that have been created for use in simulations of neat liquid water or for aqueous solution [4,5]. Most of the existing water models have been empirically parametrized to reproduce a subset of the structural and thermodynamic data available, such as radial distribution functions, heat of vaporization, freezing/boiling point, or dielectric constant. Agreement with experimental quantities not used to determine the model parameters may or may not be quantitative. More recent

* Corresponding author.
E-mail address: skinner@chem.wisc.edu (J.L. Skinner).

0301-0104/$ - see front matter © 2007 Elsevier B.V. All rights reserved.
doi:10.1016/j.chemphys.2007.06.043

models have been developed from high-level experimental studies on small water clusters [6,7], or completely from *ab initio* calculations [8,9]. Almost none of the existing water models have been parameterized to reproduce the *dynamical* properties of liquid water. These properties include the rate of hydrogen bond breaking/formation, diffusion constant, rotational correlation times, and spectral densities of low-frequency intermolecular modes (such as librations and hydrogen bond vibrations). An accurate description of these properties would seem to be essential in order to make quantitative predictions for processes where the dynamics of the solvent plays an important role.

Much of our microscopic information about liquid water comes from neutron scattering [10,11] and X-ray diffraction [12,13], X-ray absorption and X-ray Raman scattering [14,15], dielectric relaxation [16], and nuclear magnetic resonance (NMR) [17,18]. Vibrational spectroscopy provides a complementary technique to access structural and dynamical information about bulk liquid water. This technique can be particularly illuminating when the liquid has been isotopically labeled so as to eliminate difficulties due to intermolecular vibrational coupling. For example, in the case of the OD stretch of dilute HOD in H_2O, vibrational observables can be interpreted in terms of simple OD stretch local modes. In this case the OD stretch frequency can be related to the solvation environment of the local mode. Since the solvation environment is continually changing in time due to equilibrium molecular dynamics, in principle vibrational spectroscopy can provide information about both the structure and dynamics in the liquid. In the case of water, however, the large breadth of the absorption spectrum dictates that the line shape is mostly inhomogeneously broadened, and hence contains little dynamical information.

Many theoretical papers have been devoted to calculations of the vibrational absorption spectrum of water (for recent examples see Refs. [19–23]). Of particular relevance herein, we note that as early as 1991 Hermansson et al. calculated a static approximation to the absorption spectrum by performing *ab initio* calculations of the OH stretch fundamental frequencies and transition dipoles for HOD/D_2O clusters, in the field of the point charges of the surrounding water molecules [24]. The clusters were taken from snapshots of a Monte Carlo simulation, and the spectrum was approximated as the distribution of frequencies weighted by the square of the transition dipoles. More recently we have developed a similar theoretical formalism to describe both the infrared and Raman spectra for both the HOD/D_2O and HOD/H_2O model systems, which includes fluctuating transition frequencies and dipoles, and motional narrowing [25,26]. Briefly, we correlate the *ab initio* calculated transition frequencies and dipoles for a number of water clusters to the projection of the electric field on the OH (OD) bond obtained from the empirical point charges located on the (solvent) water molecules. This allows us to approximate rapidly the transition frequencies and dipoles during a subsequent MD simulation. Application of this methodology to the SPC/FQ model [27] demonstrated good agreement with both experimental IR and isotropic Raman spectra over a wide range of temperatures [26]. This technique has also been applied to solutes in aqueous solution [28–32].

While linear (steady-state) spectroscopic measurements of IR and Raman spectra yield little dynamical information, recent time-resolved, ultrafast experiments have begun to appear on the HOD/D_2O and HOD/H_2O systems [33–50]. These experiments are capable of accessing the dynamical information that is hidden (in line shapes) by inhomogeneous broadening. The latest and most powerful experiments involve the three-pulse vibrational echo technique. For example, Fecko et al. carried out three-pulse echo peak shift experiments on the HOD/D_2O system, which yield high resolution dynamical information on time scales ranging from well under 100 fs to over 1 ps [41,42]. Asbury et al. measured two-dimensional infrared (2DIR) spectra of the HOD/H_2O system, which the authors analyzed in terms of a "dynamical line width" to quantify the dynamics of the liquid [43–45]. Subsequently, Loparo et al. measured 2DIR spectra of the HOD/D_2O system [46,47,50], and analyzed these results in terms of various other metrics to discern the underlying dynamics [48].

These ultrafast experiments provide new dynamical information about water, and so it seems important to test the predictions of current simulation models against these experiments. This is in fact the goal of this paper. For such a comparison we have found that for water it is essential to calculate experimental observables directly [51], rather than, for example, comparing experimental and theoretical results for an experimentally derived quantity such as the frequency time-correlation function. Thus for such a comparison one needs to calculate non-linear response functions [52], which (in the absence of making the cumulant approximation) are functions of three independent time variables. In these calculations it is also important to account for non-Condon (the transition dipole depends on the molecular environment) effects [51]. Finally, so as to allow for a quantitative comparison between theory and experiment, one needs to convolute over the experimental pulse profiles, and include vibrational relaxation phenomenologically. Others have made the connection between simulation models and these ultrafast observables [49,50,53–57], but not at this level of detail.

Of the vast numbers of existing water models, we choose to focus on a small subset that are among the most commonly utilized and computationally tractable: the SPC/E, TIP4P, SPC/FQ, TIP4P/FQ, TIP5P/E, and Dang–Chang models. An overview of the selected water models is given below.

1.1. SPC/E

The SPC/E [58] model is a rigid, non-polarizable water model that is extremely popular for MD simulation due to its simplicity. The model consists of three interaction sites, located on the oxygen and hydrogen atomic centers. The

bond length and angles differ from the experimental gas-phase geometry of water; the O–H bond lengths are set to 1 Å and the bond angle is set to a tetrahedral angle of 109.47°. This reflects the fact that the average O–H bond lengthens, and the bond angle expands, upon moving from the gas phase to solution. The SPC/E model represents a small reparameterization of the simple point charge (SPC) model [59], which was performed in order to account for the contribution of the self-energy of effective polarization to the calculated heat of vaporization. Both the original SPC and the modified SPC/E potential were parameterized to reproduce the experimental room-temperature density and heat of vaporization of liquid water, but the SPC/E model ends up producing reasonable radial distribution functions and an acceptable diffusion constant as well.

1.2. TIP4P

The TIP4P [60] model is a four-site, rigid, non-polarizable model that is also extremely popular. The fourth, off-atom, interaction site is located a small distance from the oxygen atom, along the H–O–H bisector. The inclusion of the additional interaction site improved the agreement with the experimentally measured second peak of the O–O radial distribution function. The geometry of the TIP4P model corresponds to the experimentally measured geometry of a gas-phase water monomer; that is, O–H bond lengths of 0.9572 Å and a bond angle of 104.5°. The resulting parameterization does an excellent job of reproducing the experimental room-temperature density of water, as well as the energy and enthalpy of vaporization. The model also does a reasonable job reproducing the experimental O–O radial distribution function, although the peak positions are somewhat shifted to slightly smaller distances compared with experimental measurements [10,11]. In terms of computational efficiency, the model fares quite well. Although an additional interaction site is introduced, the number of required distance calculations per water–water interaction increases only from 9 (in the case of a three-site model) to 10; thus, the additional computational burden is not great.

1.3. TIP5P/E

The TIP5P/E [61] model is a reparameterization of the TIP5P model [62], which was very slightly modified to account for the use of the Ewald summation for long-range electrostatics in the MD simulation; the original TIP5P model was instead parameterized for use with long-range cutoffs. Both the TIP5P and TIP5P/E models are rigid, non-polarizable, five-site models, with two off-atom interaction sites located at the oxygen 'lone-pair' tetrahedral positions. The nuclear positions are in the TIP4P geometry. The TIP5P/E model was parameterized to reproduce directly the experimental O–O radial distribution function. In addition, the model was parameterized to reproduce the density and energy of water over a wide range of temperatures, from −40 to 100 °C; additionally, the model reproduces the experimentally measured density maximum around 4 °C.

1.4. SPC/FQ

The SPC/FQ [27] model is a rigid, polarizable variant of the popular SPC/E model. Unlike the original SPC/E model, the atomic charges on each water molecule can fluctuate in response to its changing electrostatic environment. In particular, the 'electro-negativity equalization' principle is used to calculate the value of each of the atomic charges at each time step. Such a polarizable model could be expected to have significant advantages over similar, non-polarizable models. Whereas non-polarizable models must account for an effective averaged polarization, which hinders their transferability, polarizable models could have the ability to reproduce data over a wide variety of thermodynamic state points. The SPC/FQ model was parameterized to reproduce directly the experimental gas-phase dipole moment, as well as radial distribution functions, and the energy and pressure of liquid water. The model also does a reasonable job of reproducing other quantities such as the NMR and Debye relaxation times. One particular shortcoming of the SPC/FQ model is its inability to describe out-of-plane polarization, due to the fact that all of the SPC/FQ charges lie in the plane of the molecule. In contrast, the experimentally measured polarizability of water is almost spherically symmetric [63].

1.5. TIP4P/FQ

The TIP4P/FQ [27] model is a rigid, polarizable variant of the popular TIP4P model. It is the fluctuating charge analogue of the TIP4P model, in the same way that SPC/FQ is the fluctuating charge analogue of the SPC/E model. The TIP4P/FQ model was parameterized to reproduce directly the experimental gas-phase dipole moment, as well as radial distribution functions and the energy and pressure of liquid water. The model also does a excellent job of reproducing other quantities such as the NMR and Debye relaxation times and dielectric constant. The diffusion constant predicted by the model is slightly too low, but nevertheless an improvement over the original TIP4P model, which yielded a diffusion constant that was too high.

1.6. Dang–Chang

The Dang–Chang model [64] is also a rigid, polarizable, four-site model, similar to the TIP4P model. Like TIP4P, the model is based on the experimental gas-phase water geometry and contains an off-atom interaction site located on the H–O–H bisector. Unlike TIP4P, however, the model includes a point polarizability on the fourth site, which results in a potential that is no longer pairwise additive. The model was extensively parameterized to reproduce not only liquid-state properties, including density, enthalpy of vaporization, liquid-state dipole, diffusion constant, and

radial distribution functions, but also energetic and geometric information from small water clusters. Thus, the model can be expected to show reasonable properties over a wide range of densities and temperatures spanning from the gas phase to the dense liquid [64,65].

In this paper we calculate both the linear (infrared absorption and isotropic Raman scattering line shapes), and non-linear ultrafast (three-pulse vibrational echo) spectroscopic observables for each of these water models. We fully account for non-Condon effects and relevant experimental parameters, so as to allow for a quantitative comparison between theory and experiment. Cognizant that errors in the structure (rather than dynamics) of the models will affect the calculated experimental observables, we also employ a normalization technique that we believe allows us to focus on dynamical differences between the models, while minimizing differences that originate from small differences in the predicted water structure. Based on these results, we reach general conclusions about which of the models seem to reproduce best the experimentally measured water dynamics.

2. Calculation of line shapes and echoes

For both the HOD/H_2O and HOD/D_2O systems, we will consider infinitely dilute HOD, with a single relevant OH or OD vibrational mode. This local mode has high frequency compared to kT, and so we will treat it quantum mechanically. All other degrees of freedom will be treated classically. This (anharmonic) local mode has vibrational eigenstates labeled $0, 1, 2\ldots$ For a given configuration of the classical degrees of freedom, the local mode has a fundamental transition frequency denoted by ω_{10}, and a transition dipole moment $\vec{\mu}_{10}$. If the electric field of all incident pulses of radiation is polarized in the $\hat{\epsilon}$ direction, and detection is in the $\hat{\epsilon}$ direction as well, then the only relevant quantity is the projection of the transition dipole along the field direction: $\mu_{10} \equiv \vec{\mu}_{10} \cdot \hat{\epsilon}$. Variations in μ_{10} from changes in the classical degrees of freedom can come from changes in the magnitude of $\vec{\mu}_{10}$ (non-Condon effects), and from changes in the angle that $\vec{\mu}_{10}$ makes with $\hat{\epsilon}$ (rotations).

2.1. Infrared and isotropic Raman line shapes

Within the mixed quantum-classical approximation described above the infrared absorption line shape for the OH (OD) stretch is given by [25,26,52]

$$I(\omega) \sim \int_{-\infty}^{\infty} \mathrm{d}t\, \mathrm{e}^{-\mathrm{i}\omega t} \left\langle \mu_{10}(0)\mu_{10}(t) \exp\left[i \int_0^t \omega_{10}(t) \right] \right\rangle \mathrm{e}^{-|t|/2T_1}. \tag{1}$$

The brackets denote a classical equilibrium statistical mechanical average, and T_1 is the lifetime of the first excited vibrational state: $T_1 = 700\,(1450)$ fs for the OH (OD) stretching mode of HOD in D_2O (H_2O) [42,43]. The line shape is related to the absorption cross section $\sigma(\omega)$ by [66]

$$\sigma(\omega) \sim \omega I(\omega). \tag{2}$$

Similarly, the isotropic Raman line shape is given by [26,66]

$$I(\omega) \sim \int_{-\infty}^{\infty} \mathrm{d}t\, \mathrm{e}^{-\mathrm{i}\omega t} \left\langle \alpha_{10}(0)\alpha_{10}(t) \exp\left[i \int_0^t \omega_{10}(t) \right] \right\rangle \mathrm{e}^{-|t|/2T_1}, \tag{3}$$

where α_{10} is the matrix element of the isotropic polarizability operator. The line shape is related to the scattering intensity $S(\omega)$ by [66]

$$S(\omega) \sim (\omega_{\mathrm{E}} - \omega)^4 I(\omega), \tag{4}$$

where ω_{E} is the frequency of the exciting light.

2.2. Three-pulse vibrational echoes

Within the same notation as above, three-pulse echo observables can be written in terms of 3rd-order non-linear response functions [51,52], given by

$$R_1(t_3,t_2,t_1) = \left\langle \mu_{10}(0)\mu_{10}(t_1)\mu_{10}(t_1+t_2)\mu_{10}(t_1+t_2+t_3) \exp\left[i \int_0^{t_1} \mathrm{d}\tau \omega_{10}(\tau) \right] \exp\left[-i \int_{t_1+t_2}^{t_1+t_2+t_3} \mathrm{d}\tau \omega_{10}(\tau) \right] \right\rangle, \tag{5a}$$

$$R_2(t_3,t_2,t_1) = R_1(t_3,t_2,t_1), \tag{5b}$$

$$R_3(t_3,t_2,t_1) = -\left\langle \mu_{10}(0)\mu_{10}(t_1)\mu_{21}(t_1+t_2)\mu_{21}(t_1+t_2+t_3) \exp\left[i \int_0^{t_1} \mathrm{d}\tau \omega_{10}(\tau) \right] \exp\left[-i \int_{t_1+t_2}^{t_1+t_2+t_3} \mathrm{d}\tau \omega_{21}(\tau) \right] \right\rangle, \tag{5c}$$

$$R_4(t_3,t_2,t_1) = \left\langle \mu_{10}(0)\mu_{10}(t_1)\mu_{10}(t_1+t_2)\mu_{10}(t_1+t_2+t_3) \exp\left[-i \int_0^{t_1} \mathrm{d}\tau \omega_{10}(\tau) \right] \exp\left[-i \int_{t_1+t_2}^{t_1+t_2+t_3} \mathrm{d}\tau \omega_{10}(\tau) \right] \right\rangle, \tag{5d}$$

$$R_5(t_3,t_2,t_1) = R_4(t_3,t_2,t_1), \tag{5e}$$

$$R_6(t_3,t_2,t_1) = -\left\langle \mu_{10}(0)\mu_{10}(t_1)\mu_{21}(t_1+t_2)\mu_{21}(t_1+t_2+t_3) \exp\left[-i \int_0^{t_1} \mathrm{d}\tau \omega_{10}(\tau) \right] \exp\left[-i \int_{t_1+t_2}^{t_1+t_2+t_3} \mathrm{d}\tau \omega_{21}(\tau) \right] \right\rangle, \tag{5f}$$

$$R_7(t_3,t_2,t_1) = \left\langle \mu_{10}(0)\mu_{21}(t_1)\mu_{21}(t_1+t_2)\mu_{10}(t_1+t_2+t_3) \exp\left[-i \int_0^{t_1+t_2+t_3} \mathrm{d}\tau \omega_{10}(\tau) \right] \exp\left[-i \int_{t_1}^{t_1+t_2} \mathrm{d}\tau \omega_{21}(\tau) \right] \right\rangle, \tag{5g}$$

$$R_8(t_3,t_2,t_1) = -\left\langle \mu_{10}(0)\mu_{21}(t_1)\mu_{10}(t_1+t_2)\mu_{21}(t_1+t_2+t_3) \exp\left[-i \int_0^{t_1+t_2} \mathrm{d}\tau \omega_{10}(\tau) \right] \exp\left[-i \int_{t_1}^{t_1+t_2+t_3} \mathrm{d}\tau \omega_{21}(\tau) \right] \right\rangle, \tag{5h}$$

where μ_{21} is the projection of the 2-1 transition dipole along the electric field unit vector, and ω_{21} is the fluctuating 2-1 transition frequency.

Vibrational relaxation is accounted for phenomenologically by multiplying these non-linear response functions by appropriate factors. Using a harmonic scaling relation to estimate the (unknown) lifetime of the second excited state [67], the appropriate multiplicative factors are given in Table 1 [42,68]. Note that since the lifetime of the second excited state is relevant only during the coherence period t_3, which is very short, it is not essential to have an accurate value for this lifetime.

The three-pulse echo is generated by exposing the sample to a sequence of three resonant pulses with wavevectors $\vec{k}_1$, $\vec{k}_2$, and $\vec{k}_3$ and frequencies ω_1, ω_2, and ω_3. The time delay between the first two pulses is τ, between the second two pulses is denoted as T, and the time after the third pulse is given by t. The resulting signal is observed in the $\vec{k}_s = -\vec{k}_1 + \vec{k}_2 + \vec{k}_3$ phase-matching direction.

The integrated echo signal, $I(\tau, T)$, is calculated by integrating the square of the electric field in the $\vec{k}_s$ direction, $E^{(3)}(\vec{k}_s, t; \tau, T)$, over t:

$$I(\tau,T) \sim \int_0^\infty \mathrm{d}t |E^{(3)}(\vec{k}_s,t;\tau,T)|^2 \sim \int_0^\infty \mathrm{d}t |P^{(3)}(\vec{k}_s,t;\tau,T)|^2, \quad (6)$$

where the polarization $P^{(3)}(\vec{k}_s, t; \tau, T)$ is given by [52]

$$P^{(3)}(\vec{k}_s,t;\tau,T) = \left(\frac{i}{\hbar}\right)^3 \sum_{j=1}^{3} \int_0^\infty \mathrm{d}t_3 \int_0^\infty \mathrm{d}t_2 \int_0^\infty \mathrm{d}t_1 \times R_j(t_3,t_2,t_1) E_3(t-t_3) E_2(t+T-t_3-t_2) \times E_1^*(t+T+\tau-t_3-t_2-t_1) \times \exp[i(\omega_3+\omega_2-\omega_1)t_3 + i(\omega_2-\omega_1)t_2 - i\omega_1 t_1], \quad (7)$$

where E_i is the experimental pulse profile for the ith pulse.

The above expression for the polarization assumes that the pulses are well separated in time, and that all delay times are positive; thus it is valid only for τ, T, and t larger than the pulse durations. Similar expressions, involving contributions from the remaining non-linear response functions, can be written down for situations where either of these assumption is violated [68]. The "echo peak shift", $\tau^*(T)$, is defined to be the value of τ that maximizes the integrated echo signal for a given value of waiting time, T.

The vibrational echo signal can also by measured via heterodyne detection, whereby the emitted signal is mixed with a strong local oscillator pulse, with electric field denoted E_{LO}. The difference signal resulting from the sample (the difference between the mixed local oscillator/echo signal and isolated local oscillator) is then given by [52]

$$I(\tau,T,\tau') = -2\mathrm{Im} \int_{-\infty}^{\infty} \mathrm{d}t E_{\mathrm{LO}}^*(t-\tau') P^{(3)}(\vec{k}_s,t;\tau,T) \times \exp[i(\omega_{\mathrm{LO}} - \omega_3 - \omega_2 + \omega_1)t]. \quad (8)$$

The 2DIR spectrum is calculated from the real part of the Fourier transform of the above signal over the τ and τ' dimensions (with frequencies ω_1 and ω_3); this is equivalent to summing the individual one-sided Fourier transforms of the rephasing and non-rephasing signals, as described previously [51]. The "dynamic line width," $\Gamma(T)$, is defined to be the FWHM of a one-dimensional slice through the maximum of the two-dimensional 0-1 resonance, along the ω_1 axis for a particular waiting time T [43–45]. The "nodal slope" is a complementary metric to the dynamic line width, and provides an alternative way to quantify the inherently two-dimensional information contained in the 2DIR spectrum [50]. The nodal slope is defined to be the slope of the node separating the positive-going 0-1 and negative-going 1-2 resonances in the two-dimensional spectrum. As correlation is lost as a function of T, between the frequencies in the τ and t periods, the 0-1 and 1-2 resonances become more circular, and the slope of the nodal line goes to zero. Thus, the nodal slope is a measure of the residual frequency correlation, and thus a measure of the dynamics.

Table 1
Summary of relaxation factors for the non-linear response functions [68]

Response functions	Factor
R_1, R_2, R_4, R_5, R_7	$e^{-(t_3+2t_2+t_1)/2T_1}$
R_3, R_6, R_8	$e^{-(3t_3+2t_2+t_1)/2T_1}$

2.3. Calculation of frequencies and transition dipoles

To calculate the line shapes and non-linear response functions, one needs time-dependent trajectories of transition frequencies and dipoles. As we have done before [25,26,30,51,56], we will utilize the empirical frequency correlation (EFC) method in order to calculate the required quantities. Briefly, the EFC technique begins by sampling solute/solvent clusters from an MD simulation, and using *ab initio* techniques to calculate the frequencies and transition dipoles of the solute in the presence of the solvent. An empirical correlation is then derived between the *ab initio* calculated frequencies and transition dipoles, and the external electric field generated by the point charges on the surrounding water molecules. This correlation thus provides a computationally efficient way to estimate the instantaneous transition frequencies and dipoles of a solute during a subsequent MD simulation. Complete details of the procedure are available elsewhere [25,26,51].

We first apply the EFC method to the SPC/E water model, as has been done in previous work [25,51]. The resulting relations between the SPC/E generated electric field, and the OH (OD) transition frequencies are given in Table 2. Note that the expressions for the transition frequencies are identical to those reported in Refs. [25,51], but differ from those reported in Ref. [26], since the latter were

Table 2
Empirical relationships for the transition frequencies, dipole (polarizability) derivatives (normalized by their gas-phase values), and matrix elements

Vibration	Empirical relationship	R	RMS error
OH	$\omega_{10} = 3806.1\ \text{cm}^{-1} - 10792\ \text{cm}^{-1}/\text{au}\ E$	0.89	$65\ \text{cm}^{-1}$
	$\omega_{21} = 3631.3\ \text{cm}^{-1} - 12117\ \text{cm}^{-1}/\text{au}\ E$	0.90	$72\ \text{cm}^{-1}$
	$x_{10} = 0.1018\ \text{Å} - 0.922 \times 10^{-5}\ \text{Å}/\text{cm}^{-1}\ \omega_{10}$	0.998	5.2×10^{-5} Å
	$x_{21} = 0.1425\ \text{Å} - 1.30 \times 10^{-5}\ \text{Å}/\text{cm}^{-1}\ \omega_{21}$	0.999	9.1×10^{-5} Å
OD	$\omega_{10} = 2792.7\ \text{cm}^{-1} - 7559.5\ \text{cm}^{-1}/\text{au}\ E$	0.89	$46\ \text{cm}^{-1}$
	$\omega_{21} = 2700.6\ \text{cm}^{-1} - 8258.0\ \text{cm}^{-1}/\text{au}\ E$	0.89	$49\ \text{cm}^{-1}$
	$x_{10} = 0.08727\ \text{Å} - 1.09 \times 10^{-5}\ \text{Å}/\text{cm}^{-1}\ \omega_{10}$	0.999	3.8×10^{-5} Å
	$x_{21} = 0.1224\ \text{Å} - 1.54 \times 10^{-5}\ \text{Å}/\text{cm}^{-1}\ \omega_{21}$	0.999	6.5×10^{-5} Å
Both	$\mu'/\mu'_g = 1.177 + 71.86\ \text{au}^{-1}\ E$	0.92	0.37
Both	$\alpha'/\alpha'_g = 1.329 + 3.841\ \text{au}^{-1}\ E$	0.31	0.14

The electric field, E, at the H (D) and in the direction of the OH (OD) bond, is in au; frequencies, ω, are in cm^{-1}; and the matrix elements, x_{10} and x_{21}, are in Å. The correlation coefficient, R, and RMS error of each fit are also listed.

for the SPC/FQ model. The matrix elements of the transition dipoles are written approximately as [26]

$$\mu_{ij} = \mu' x_{ij} \hat{u} \cdot \hat{\epsilon}, \tag{9}$$

where μ' is the magnitude of the dipole derivative, $\hat{u}$ is the OH (OD) bond vector, and x_{ij} are the position matrix elements. As before, μ' is correlated with the local field, and the position matrix elements are correlated with the local mode transition frequencies. The expressions for these are also given in Table 2. Note that the expressions for the position matrix elements differ slightly from those given previously in Ref. [51], due to two factors: there is an error in the matrix element in Eq. (17) of Ref. [26]—the correct expression should read, in the notation of that paper, $x_{10} = (k-3)^{1/2}/\alpha(k-2)$; and there was an additional error in the code to calculate these matrix elements. We have verified that the results in both Refs. [26,51] are not perceptibly changed by correcting these errors, since the matrix elements are only weakly sensitive to the frequencies, and the transition dipoles are dominated by variations in μ' and $\hat{u} \cdot \hat{\epsilon}$. For the isotropic Raman spectrum the transition polarizability is similarly written as $\alpha_{10} = \alpha' x_{10}$. The correlation of α' with the electric field [26] is also given in Table 2.

Although it would be possible to apply the EFC procedure from scratch (sampling clusters, carrying out electronic structure, etc.) for each water model (which is what we have done for the TIP4P and SPC/FQ models in previous papers [25,26]), such a procedure would be very time consuming. More importantly, the imperfect correlation, for example, between field and frequency for each model would make it considerably more difficult to make a direct comparison among the water models. In fact, within the Born–Oppenheimer approximation, the transition frequencies, dipoles, etc., are functionals of the nuclear positions of the solvent molecules. Inasmuch as the electric field is a surrogate for the nuclear positions, we should be able to apply the above procedure for any other model with the SPC/E nuclear geometry. To this end, for the SPC/FQ model we can calculate the correlation with the field by assigning SPC/E charges to the atoms. We then use these charges for calculating the electric field, and thus the transition frequencies and dipoles, using the relationships given in Table 2. Note that these charges are used only for the calculation of the frequencies and transition dipoles, and *not* for the MD simulation. Thus, the structure and the dynamics of the water model is unaffected by this procedure.

The other water models have the TIP4P nuclear geometry. Again, following the logic above, it is preferable to have a single mapping from field to frequency, etc., which we can use for all the models. To this end we first transform the water molecules into the SPC/E geometry, by holding the center of mass and symmetry plane of each water molecule fixed. We then follow the above procedure to calculate the frequencies and transition dipoles (polarizabilities). Once again, the modifications of the geometry and charges are only used for the purpose of frequency calculation, and *not* for the MD simulation. Thus, the underlying water model is once again unaffected by the procedure.

By using a single correlation between the field generated from the SPC/E charges and the transition frequency, etc., we establish a uniform (although certainly not perfect) mapping between nuclear position and frequency, which allows for unbiased comparisons among all water models. Note that in doing so we are making an assumption that the clusters generated by the SPC/E model are representative of clusters that would be generated from *any* reasonable water model. Given that all the water models (approximately) reproduce the experimental radial distribution functions, this assumption seems well-founded.

2.4. Simulation details

The simulation details varied slightly for each water model, since some of the codes were provided by the creators of the model. In general, all simulations were performed with between 108 and 128 water molecules, with the size of the cubic simulation box chosen to give the number density of normal or heavy water at the temperature of

the simulation [69]. Periodic boundary conditions were employed, and the electrostatic forces were calculated using the Ewald summation. The systems were equilibrated at 300 K, and the equations of motion were propagated using 0.5 fs time steps.

Our simulations are actually of the neat liquids H_2O or D_2O rather than specifically of HOD in H_2O or D_2O. By simulating the neat liquid we have over 200 independent local modes of vibration rather than just one (i.e. we can presume that each bond in the system is the local oscillator of interest). The effects of this approximation on the dynamics of the system have been verified to be negligible [25].

During the course of the MD simulation, frequency and transition dipole (polarizability) trajectories were calculated for each local mode at each MD step using the equations found in Table 2. Each of the six unique semi-classical response functions was numerically sampled for 2.4 ns, utilizing the Wiener–Khintchine theorem as described in Ref. [51]. The results were saved for subsequent calculation of the relevant spectroscopic observables.

3. Results and discussion

3.1. IR and Raman line shapes

The calculated normalized IR line shapes for the HOD/D_2O system are given in Fig. 1[1], and compared to the experimental results from Ref. [42]. The latter are obtained from the experimental cross section using Eq. (2), and then normalizing. It is apparent that all models yield IR line shapes that are too red-shifted as compared to the experimentally measured line shape. Most of the models have widths reasonably close to experiment, but the Dang–Chang line shape is too narrow. The relevant spectroscopic parameters (peak shifts from the gas-phase value of 3707 cm^{-1} and FWHM widths) are given in Table 3.

Moving on to a comparison of the Raman line shapes of the same system, experimental (results are from Ref. [70], corrected by Eq. (4), using the appropriate ω_E for Ar ion laser excitation) and theoretical line shapes are shown in Fig. 2. (Note that the experimental line shape is from the unpolarized signal, whereas the theoretical result is for the isotropic line shape; in this particular instance, however, the difference between these two is quite small [71,72].) First of all one sees that the line shapes (theoretical and experimental) are all somewhat less red-shifted than their IR counterparts. Second, one sees a pronounced shoulder on the blue side of the band in both theory and experiment, although the shoulder is more prominent in the theory for most of the models (especially SPC/FQ and TIP5P/E). This shoulder has previously been attributed to the sub-population of molecules whose H atom is not hydrogen bonded [73]. The red shift of the IR (compared to the Raman) line shape, and the suppression of the shoulder, are both direct results of the non-Condon effects in the system [26], whereby the transition dipoles on the red side of the band are significantly larger than those on the blue side. Thus, the contribution from those oscillators on the red side of the band is significantly enhanced in the IR line shape, increasing the red shift of the line shape and decreasing the relative magnitude of the shoulder on the blue side of the band. In contrast, the transition polarizability, relevant to the Raman line shape, changes only marginally across the band [26]. The theoretical Raman line shapes have too much intensity above 3700 cm^{-1}. In general, most of the models give reasonably accurate predictions for the width of the Raman line shape, with the notable exception of SPC/FQ, which predicts a width that is somewhat too large, and Dang–Chang, which once again predicts a width that is considerably too small. The relevant spectroscopic parameters are again summarized in Table 3.

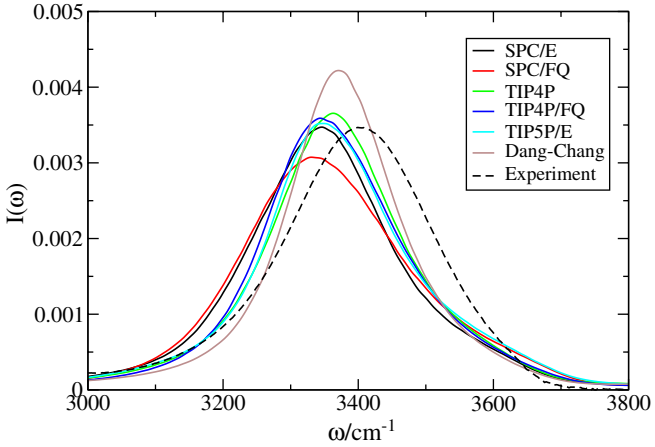

Fig. 1. Calculated IR line shapes for the HOD/D_2O system. The experimental line shape is from Ref. [42].

The calculated IR and Raman line shapes for the HOD/H_2O system are shown in Figs. 3 and 4, alongside the corresponding experimental results [43,70]. As with the case of D_2O, all models predict IR line shapes that are slightly too red-shifted, but the widths are about right (except SPC/FQ, which is too broad, and Dang–Chang, which is quite a bit too narrow). The situation with the Raman line shape is similar. As above, most of the theoretical Raman line shapes have shoulders on the blue side that are too pronounced, and extend too high in frequency. The relevant spectroscopic parameters for both the IR and Raman line shapes are summarized in Table 3 (the gas-phase value of the OD stretch frequency in HOD is 2724 cm^{-1}).

Discrepancies between the calculated and experimental IR and Raman line shapes can be interpreted in terms of differences in the underlying distributions of frequencies found in the liquid, $P(\omega)$ (an equilibrium property, determined by the structure of the liquid), and/or the dynamics

[1] For interpretation of color in the figures, the reader is referred to the web version of this article.

Table 3
Summary of IR and Raman peak shifts and FWHM line widths for the different water models

Model	System	$P(\omega)$			IR		Raman	
		$\langle\omega\rangle$	σ	FWHM	Shift	FWHM	Shift	FWHM
SPC/E	H_2O	2522	99	267	−246	150	−236	164
SPC/FQ	H_2O	2509	107	302	−258	177	−244	212
TIP4P	H_2O	2531	95	254	−238	140	−229	156
TIP4P/FQ	H_2O	2531	99	245	−251	146	−232	171
TIP5P/E	H_2O	2537	102	278	−244	136	−232	160
Dang–Chang	H_2O	2530	88	215	−232	117	−225	128
Experiment	H_2O	–	–	–	−214[a]	159[a]	−201[b]	175[b]
SPC/E	D_2O	3418	141	383	−361	231	−344	260
SPC/FQ	D_2O	3438	155	437	−376	272	−345	361
TIP4P	D_2O	3430	135	353	−344	215	−325	251
TIP4P/FQ	D_2O	3436	141	356	−362	226	−337	271
TIP5P/E	D_2O	3444	146	400	−359	218	−333	281
Dang–Chang	D_2O	3431	126	304	−336	186	−323	205
Experiment	D_2O	–	–	–	−300[c]	254[c]	−270[b]	279[b]

Also listed are the average $\langle\omega\rangle$, standard deviation σ, and FWHM for each frequency distribution. All results are in cm^{-1}.
[a] Ref. [43].
[b] Ref. [70].
[c] Ref. [42].

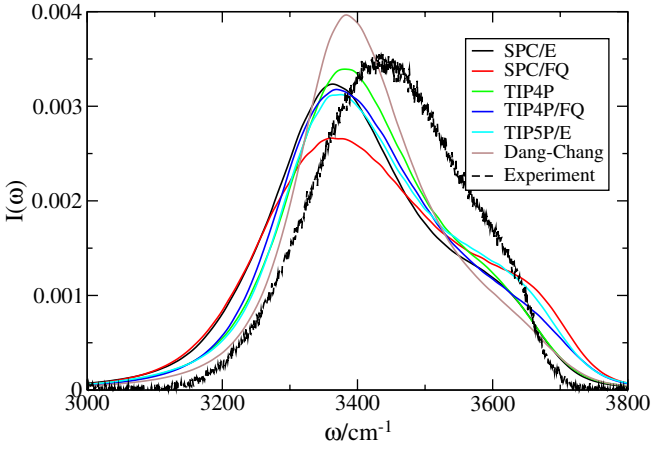

Fig. 2. Calculated Raman line shapes for the HOD/D_2O system. The experimental line shape is from Ref. [70].

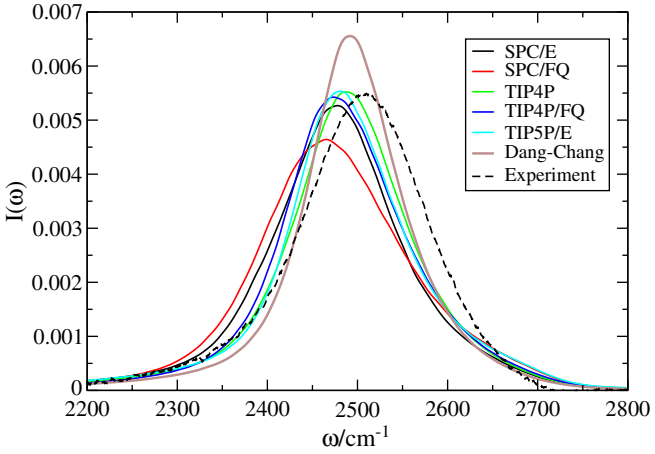

Fig. 3. Calculated IR line shapes for the HOD/H_2O system. The experimental line shape is from Ref. [43].

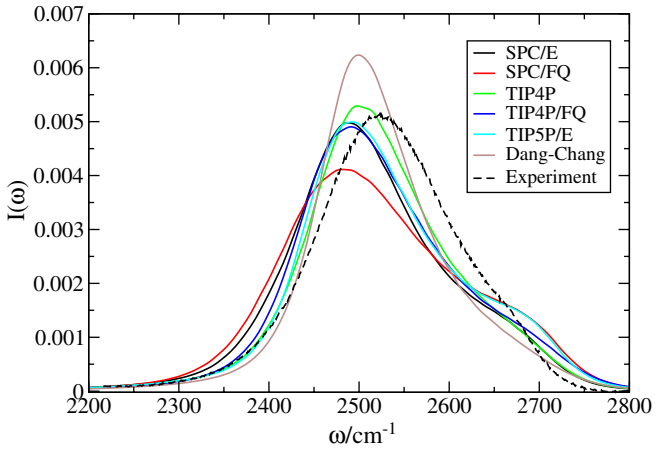

Fig. 4. Calculated Raman line shapes for the HOD/H_2O system. The experimental line shape is from Ref. [70].

of the liquid. In this case, however, because the distribution of frequencies is so wide (compared to the inverse of the frequency fluctuation correlation time), the IR and Raman line shapes in water are determined to a large extent by the distribution of frequencies alone; that is, there is not a huge amount of motional narrowing [20]. In order to understand better the differences in the calculated IR and Raman line shapes, the distributions of frequencies are plotted in Figs. 5 and 6. Not surprisingly, the underlying frequency distributions mirror the same trends found in the IR and Raman line shapes. In general, the distributions of frequencies resulting from the SPC/FQ model are the broadest, and those from the Dang–Chang model are the narrowest. The distributions all show distinct shoulders on the blue side of the band, with those from the SPC/FQ and TIP5P/E models being especially pronounced. In general,

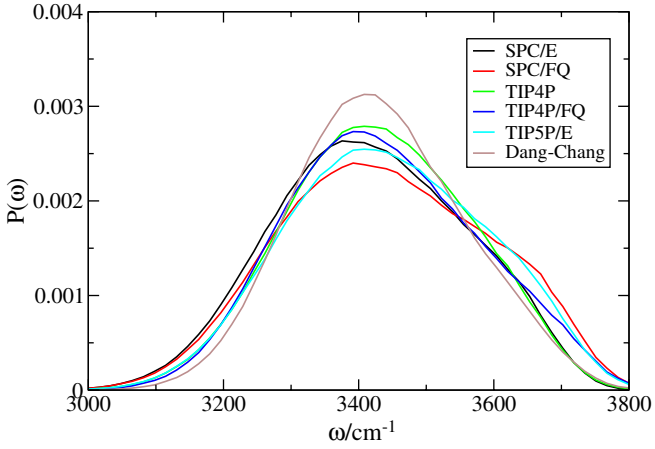

Fig. 5. Calculated frequency distributions for the HOD/D_2O system.

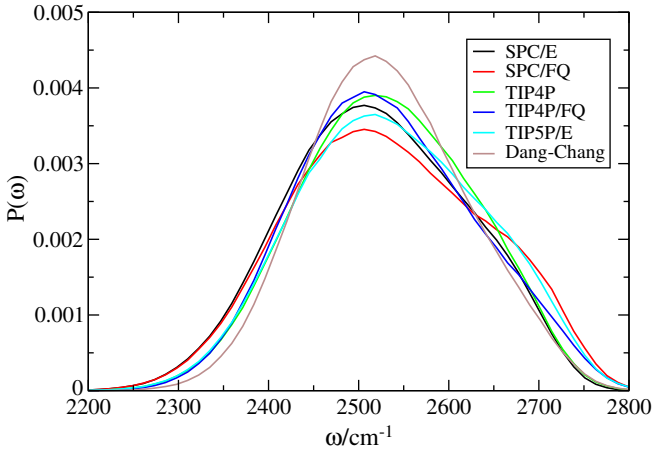

Fig. 6. Calculated frequency distributions for the HOD/H_2O system.

the distributions for the SPC/E, TIP4P, TIP4P/FQ, and TIP5P/E models are very similar. The statistical properties of these distributions are summarized in Table 3.

As a static property, the distribution of frequencies is completely determined by the structure of the liquid. In particular, since the OH (OD) stretch frequency is to a large extent determined by the distance of the closest oxygen atom [53,73], it makes sense to attempt to ascribe the differences in the calculated distribution of frequencies to differences in the intermolecular O–H (O–D) radial distribution function, $g_{OH}(r)$. These distribution functions for the various models are shown in Fig. 7, alongside the most recent experimental results of Soper [11].

It is evident from the figure that there is considerable variation among the predictions of the various water models, in terms of the position, height, and width of the first and second (intermolecular) peaks, consistent with the observed variability in the calculated frequency distributions. It is also evident that *all* of the models exhibit first peaks that are considerably too tall and narrow as compared to the experimental results of Soper. The explanation for these discrepancies is primarily the result of two factors.

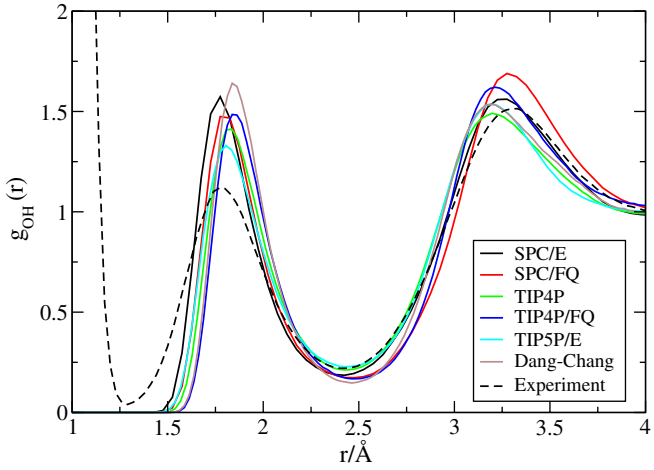

Fig. 7. Calculated O–H radial distribution functions. The experimental distribution is from Ref. [11].

First, the majority of these models were parameterized against (or at least compared to) the older, presumably less accurate, neutron scattering data of Soper and Phillips [10]. $g_{OH}(r)$ from this data shows a significantly higher first peak, and thus would indicate significantly better agreement with the simulation results. Secondly, there is the issue of nuclear quantum effects. The classical models of course have no quantum effects (although through their comparison/parameterization to experiment, some of these quantum effects are incorporated in an effective manner). Rossky, Berne and coworkers [74–76] have demonstrated that including quantum effects into a classical water model leads to a considerable decrease in the height and increase in the breadth of the first intermolecular peak of $g_{OH}(r)$, although the peak is generally still slightly too narrow as compared to the new experimental results of Soper. So to some extent the discrepancy in the widths of the first peak must be due to these nuclear quantum effects (in this case the quantum dispersion of the light hydrogen atom). It is possible that reparameterization of some of these classical models might be able to describe these effects, but probably only at the expense of experimental/theoretical agreement of other properties. It is also important to note that the discrepancy between theory and simulation in the first peak is not necessarily reflected in the discrepancies in the spectra, because for the latter nuclear quantum effects *are* included. That is, the adiabatic scanning procedure that we use to calculate the transition frequencies explicitly takes the quantum dispersion of the hydrogen atom into account, at least in the radial direction, since its intramolecular vibrational motion is treated purely quantum mechanically.

3.2. Three-pulse vibrational echoes

Since we have established that the differences among the theoretical IR and Raman line shapes can be largely attributed to differences in the predicted water structure for each

water model, and that these line shapes are relatively insensitive to the water dynamics, it is difficult to assess the accuracy of the dynamics of these models based on these results. At this point, therefore, we turn to the non-linear ultrafast spectroscopic observables, which in turn are much more sensitive probes of dynamics than are the linear steady-state measurements. The quantities that we choose to calculate will be motivated in large part by the availability of corresponding experimental measurements, and thus we will consider different quantities for the H_2O and D_2O systems.

Turning our attention first to the HOD/D_2O system, the first experimental results reported were for the integrated echo [41]. As discussed above, all excitation and detection electric fields in the experiment were parallel. We calculate this integrated echo intensity as described above, for the six different simulation models. In these calculations, the excitation pulses were centered at 3275 cm^{-1} (as in experiment [41,42]), which is midway between the 1-0 and 2-1 resonances. The experimental pulse envelopes for the electric field were non-Gaussian, with a FWHM of 52 fs [42]. For simplicity we modeled this situation with Gaussian pulses with the same FWHM, or equivalently, the (Gaussian) pulses at the intensity level had a FWHM of 37 fs. The resulting three-pulse echo peak shifts are shown alongside the experimental results of Tokmakoff and coworkers [42] in Fig. 8. One sees good qualitative agreement between theory and experiment for all models, for both the initial value and the subsequent time evolution. The best quantitative agreement at short times comes from the TIP4P and TIP5P/E models, in terms of the initial peak shift and the recurrence at 100–200 fs. Primarily on the basis of molecular dynamics simulations the latter has been attributed to the underdamped hydrogen bond stretch [20,41,53,55,57,73,77]. The SPC/E and Dang–Chang models also show this recurrence, while the FQ models do not. In terms of the longer-time decay, it appears that the polarizable models more accurately describe the experimental situation

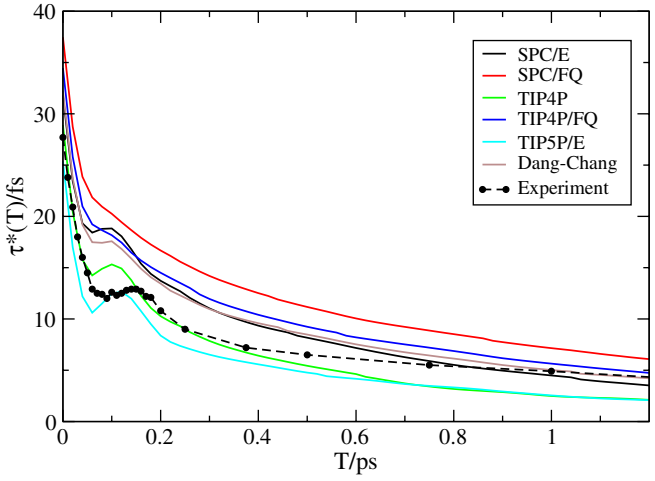

Fig. 8. Calculated echo peak shifts for the HOD/D_2O system. The experimental peak shifts are from Ref. [42].

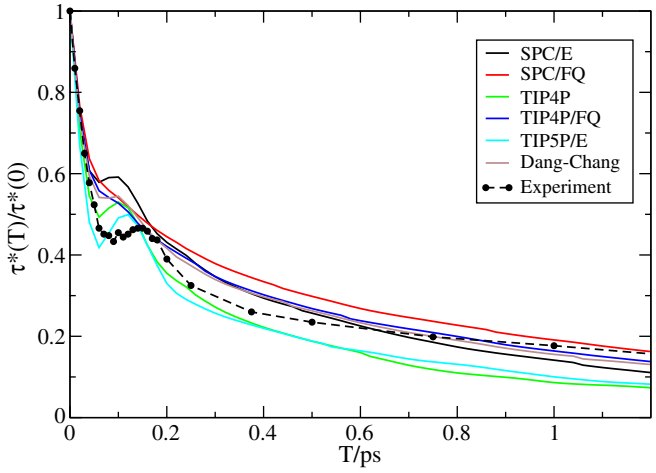

Fig. 9. Normalized echo peak shifts for the HOD/D_2O system.

[51]. The long-time decay has been attributed to hydrogen bond making and breaking, or to electric field fluctuations arising from collective hydrogen bond reorganization [35,49,50,53,57,73,77].

Since the initial peak shift is largely determined by the width of the distribution of frequencies and/or lineshape, which we know to be relatively insensitive to dynamics, we also plot the normalized peak shift in Fig. 9. That is, for both experiment and theory we divide by the corresponding initial value. This goal here is not to make the theoretical results look better, but rather it is an attempt to focus more on the dynamics. This plot emphasizes the qualitative agreement at short times of all models except FQ with experiment, and the fact that all models, especially TIP4P and TIP5P/E, decay too quickly at long times.

We can also calculate the 2DIR spectrum as a function of the waiting time, T, as described above. Parameters for the pulses are identical to those given above. Examples of such calculated spectra, for the SPC/E model, are shown in Fig. 10 for several selected waiting times. These spectra can be compared to the experimentally measured spectra taken by Tokmakoff and coworkers [46,47,50]. In order to make a quantitative comparison between theory and experiment for these two-dimensional data, a number of different procedures have been proposed that reduce in some manner or another to one-dimensional projections [48]. One example is the "nodal slope", S, which is the slope of the (approximate) straight line separating the positive-going 1-0 resonance from the negative-going 2-1 resonance. Although there is probably no particular reason to

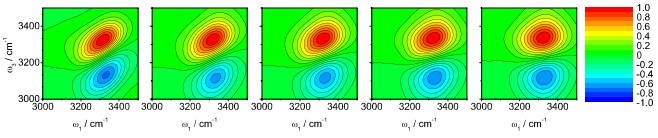

Fig. 10. Calculated 2DIR spectra for the SPC/E water model and the HOD/D_2O system. The spectra correspond to waiting times $T = 0$, 100, 200, 400 and 800 fs, respectively.

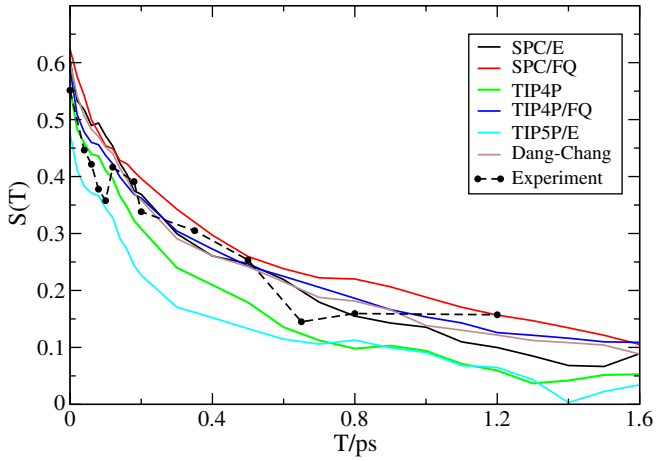

Fig. 11. Calculated nodal slopes for the HOD/D_2O system. The experimental results are from Ref. [50].

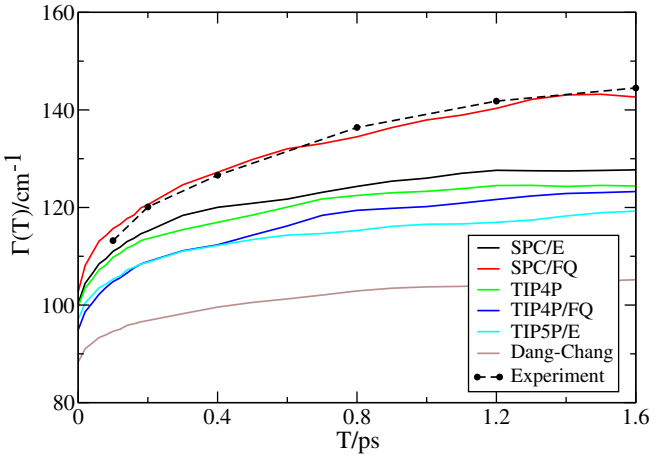

Fig. 13. Calculated dynamic line widths for the HOD/H_2O system. The experimental dynamic line width is from Ref. [45].

choose this procedure over others [48], experimental results for the nodal slope were reported for this system by Eaves et al. [50]. Thus for each of the simulation models we show the nodal slope as a function of waiting time, in Fig. 11. Also shown is the nodal slope as extracted from the 2DIR experimental results of Tokmakoff and coworkers [50]. Nodal slopes extracted from the data in Ref. [46] are qualitatively similar, but are smaller (for each value of T) by up to 0.15. The most prominent features of the experimentally measured nodal slope are a rapid decay of the slope within 100 fs, followed by an oscillation at about 150 fs, and a final, slower, decay. The theoretical results of all models except TIP5P/E and TIP4P, whose nodal slopes are likely to be too small (it is not possible to say anything more definite without experimental error bars), are in reasonable agreement with the experimental data, although none of the theoretical curves shows the oscillation.

We now turn our attention to the HOD/H_2O system. 2DIR experiments on this system were reported by Fayer and coworkers [43–45]; analogous integrated echo experiments have not been performed. As above, excitation and detection was in the all-parallel configuration. The theoretical pulse profiles in this case are as in the corresponding experiment: Gaussians, centered at 2500 cm^{-1} with a FWHM (at the intensity level) of 51 fs. Examples of such calculated spectra, for the SPC/E model, are shown in Fig. 12 for several selected waiting times. These spectra can be compared to the experimentally measured spectra

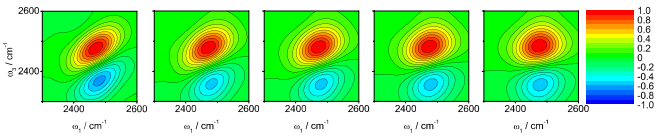

Fig. 12. Calculated 2DIR spectra for the SPC/E water model and the HOD/H_2O system. The spectra correspond to waiting times $T = 0$, 100, 200, 400 and 800 fs, respectively.

taken by Asbury et al. [45]. These authors have quantified their measured spectra in terms of a different one-dimensional projection, the "dynamic line width" (DLW), which is the FWHM of a cross section of the 1-0 resonance taken through its maximum. The DLWs for the different simulation models, and the experimental results, are shown in Fig. 13. The agreement between experiment and theory for the SPC/FQ model is quite remarkable, while results for the other models are not in very good agreement.

In the impulsive limit (infinitely short pulses), the DLW asymptotically approaches the FWHM of the linear spectrum as the waiting time, T, becomes long [51]. However, when finite pulses are used, the DLW does not approach the FWHM of the linear spectrum, but rather approaches a narrower value that is dependent on the pulse profile [45]. Unfortunately, it is difficult to evaluate the dynamics of the water models from Fig. 13, since each of the models is approaching a different asymptotic limit due to differences in the linear spectra. Since we have already concluded that such differences are primarily due to structural shortcomings, it makes sense to normalize the DLW as $(\Gamma - \Gamma(T))/\Gamma$, where $\Gamma(T)$ is the DLW, with asymptotic value Γ, so as to allow for a more effective comparison of the dynamics. To this end, we present a normalized description of the same information in Fig. 14. It is difficult to make any definitive conclusions regarding the short-time dynamics of the water models based on the DLW since the first experimental data point is not taken until $T = 100$ fs. Thus, we will use this metric as a indicator of the long-time dynamics. In this regard, the FQ models do very well, consistent with our findings for the D_2O system, while the values for the other models are generally too small.

In order to make a connection between the experiments of the Tokmakoff and Fayer groups, we have calculated the nodal slopes of the 2DIR spectra for the H_2O system. The results for both theory and experiment are shown in Fig. 15. The results of the nodal slope calculation mirror those of the DLW, with relatively good agreement between

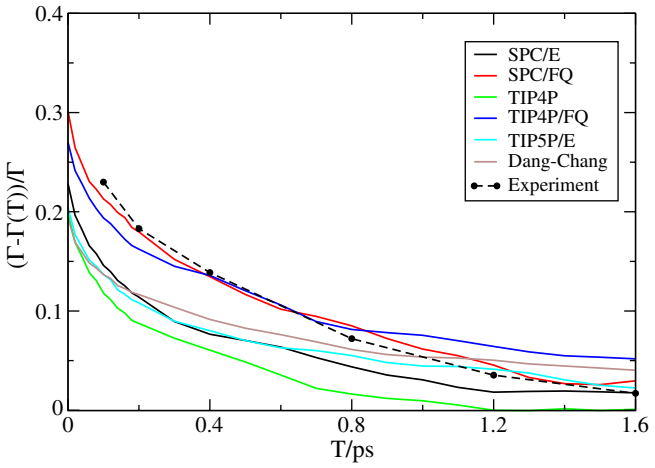

Fig. 14. Normalized dynamic line widths for the HOD/H_2O system.

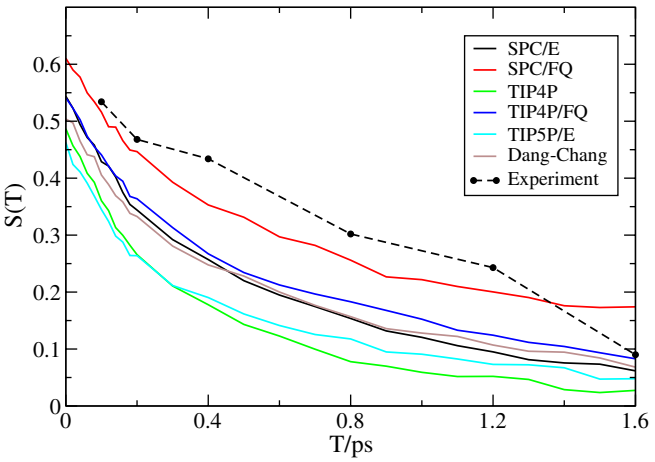

Fig. 15. Calculated nodal slopes for the HOD/H_2O system. The experimental results are from Ref. [45].

the experimental result and that of the SPC/FQ model, and to a lesser extent, the other polarizable models. The nonpolarizable TIP4P and TIP5P/E models seem to decay too fast at intermediate to long times compared to experiment. It is also interesting to note that although the theoretical nodal slopes for the two systems (D_2O and H_2O) are very similar for each model, the corresponding experimental results are less similar in that results for H_2O are somewhat larger.

Having made many comparisons to experimental spectroscopic observables, it is now insightful to examine the underlying frequency time-correlation functions (FTCFs) of the models themselves. Under the cumulant and Condon approximations, all of the previously calculated spectroscopic observables can be related to the underlying FTCF; unfortunately, both of these approximations are suspect for the D_2O and H_2O systems [26,51]. Nonetheless, the FTCFs still provide an excellent means of theoretical comparison of the underlying dynamics of the various water models. The normalized FTCFs for the H_2O system for the various models of interest are shown in Fig. 16. Since the (normalized) FTCFs for the corresponding D_2O system are essentially indistinguishable from their H_2O counterparts, the former have been omitted for clarity. The initial values of the FTCFs can be determined from the variances of the frequency distributions, given in Table 3.

The FTCFs reinforce some of the conclusions that we have already drawn regarding both the short- and long-time dynamics of the various water models. It is evident from the plot that the FQ models have dramatically different short-time dynamics than do the remaining models, as evidenced by the slower initial decay of the FTCF, the smaller initial drop, and the lack of an oscillation. Examining these curves on a logarithmic plot, it is also evident that there is a considerable difference in the long-time decay constants of the FTCFs, with the polarizable models having by far the slowest decay constants, and the TIP4P model decaying the fastest. In general, these differences are well reflected in the corresponding calculated spectroscopic observables.

It is worthwhile noting that the integrated peak shift and 2DIR experiments on HOD/H_2O and HOD/D_2O have significant differences, and hence features of the FTCF are reflected in different ways. In particular, the integrated echo experiment is homodyned, and therefore the intensity goes like the transition dipole to the eighth power, whereas

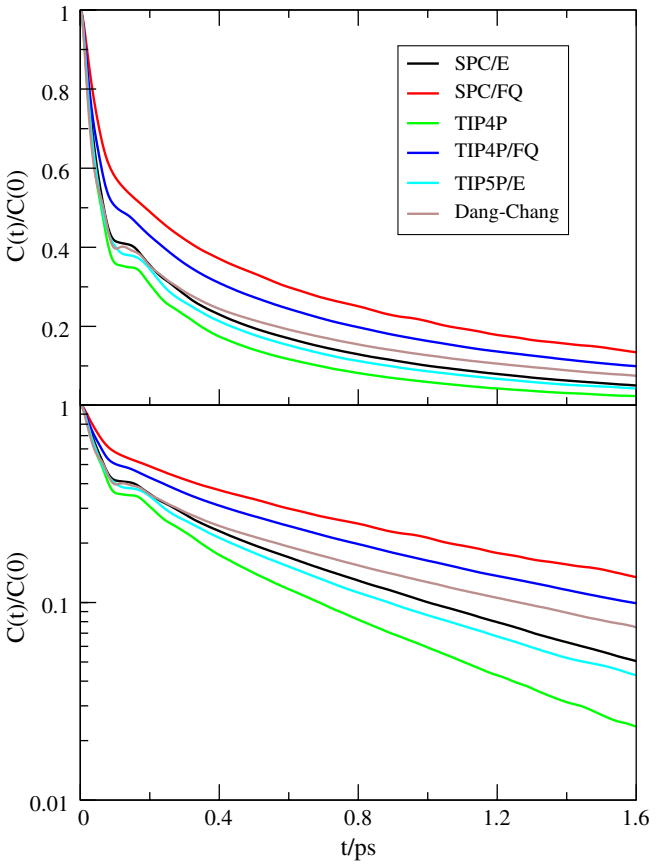

Fig. 16. Calculated FTCFs for the HOD/H_2O system. Linear (top) and logarithmic (bottom) plots.

the 2DIR experiment is heterodyned, and the amplitude goes like the transition dipole to the fourth power. Therefore the importance of non-Condon effects is emphasized in the former [51]. In the HOD/D_2O experiments the excitation pulses are centered between the 1-0 and 2-1 resonances, thereby emphasizing dynamics on the red side of the 1-0 resonance, whereas in the HOD/H_2O experiments the pulses are centered at the peak of the 1-0 resonance. Thus, for example, theoretically we find that the oscillation of the FTCF appears in the HOD/D_2O peak shift experiments, but does not appear in the nodal slopes for either system, or in the DLW for HOD/H_2O.

4. Conclusion

We have presented a detailed comparison between the theoretically calculated and experimentally measured linear and non-linear ultrafast spectroscopic observables for a variety of common water simulation models, for both the HOD/D_2O and HOD/H_2O systems. In particular, we looked at comparisons between the linear IR and Raman spectra, the three-pulse vibrational echo peak shift, and both the dynamic line width and nodal slope of the 2DIR spectra. We attempted to remove the bias due to differences in water structure among the various models through normalization, and as such have tried to reach conclusions regarding the accuracy of the dynamics predicted by the various water models compared to the true dynamics of liquid water.

Before attempting to draw some final conclusions, it is essential to understand the limitations of our theoretical results. First, the profound differences between the experimentally measured O–H radial distribution function, $g_{OH}(r)$, and those predicted by the various models (Fig. 7), means that it is essentially impossible for any of these models to make a perfect prediction of the spectroscopy of liquid water. Even though a large fraction of this difference can be attributed to quantum dispersion of the hydrogen (which is in fact taken into account to some extent by our mixed quantum-classical approach), a significant difference remains unaccounted for [74]. Secondly, the computational method used for the calculation of the frequencies and transition dipoles also necessarily involves some inaccuracies. Although we have previously used this technique with considerable success [26], for example, a detailed comparison between frequencies from our empirical approach and those obtained from *ab initio* calculations on water clusters, shows a fair amount of dispersion; see, for example, Fig. 4 of Ref. [25]. Additionally, the application of the computational technique, parameterized for clusters, to the bulk, necessarily involves some extrapolation that can also introduce systematic errors. We have attempted to mitigate the effects of these issues by applying our computational strategy uniformly to all models, such that the sources of these errors are at least constant for all models, and through the normalization scheme discussed above. In this way, we can focus on the differences among the models caused by dynamics, while hopefully minimizing the effects of any systematic errors.

With those caveats in mind, we now move to some general conclusions. In terms of the linear spectroscopic observables, the first interesting result is that SPC/FQ, while working quite well for the IR spectra, overestimates the width of the Raman spectra. This was true to a lesser extent in the previous work by Corcelli and Skinner [26], who used the same technique, but calculated the electric field from the fluctuating SPC/FQ charges, rather than from the SPC/E charges as we did here. These differences between different ways to connect a simulation model to spectroscopy, are typical of the systematic errors described above, for any one model. Additionally, we find that the Dang–Chang model yields spectra that are uniformly too narrow, a feature that is reflected in the narrow underlying frequency distribution for this model. Overall, in terms of the linear spectra, it seems that the SPC/E and TIP4P models makes the most reasonable predictions for the spectra, and do particularly well in the Raman calculations; the SPC/E model generally makes more accurate predictions for the spectral width, while the TIP4P model makes the more accurate predictions regarding the shift.

Turning to the echo peak shift calculations on the D_2O system, we find that the FQ models lack the prominent oscillation that is found in the experimentally measured peak shift, while the remaining models all display an oscillation of varying amplitude. The TIP4P and TIP5P/E models seem to display the best agreement at short times in terms of initial decay and the oscillation, but then decay too fast with respect to experiment at long time. The polarizable FQ and Dang–Chang models seem most accurate at longer times. The TIP4P and TIP5P/E models perform least well in the nodal slope calculations for the D_2O system. Looking at the DLW and nodal slope calculations for the H_2O system, in both cases the SPC/FQ model does quite well, with excellent agreement with the experimentally measured DLW even before scaling! The TIP4P/FQ model also yields reasonable agreement with the DLW, but does not fare as well as SPC/FQ in the nodal slope calculation. The TIP4P model displays the worst agreement in both cases.

Before reaching some final conclusions regarding the accuracy of the dynamics from each of these models of liquid H_2O, it is useful to discuss the results of some previous calculations of some other dynamic and equilibrium properties of these models. In particular, we will consider the diffusion constant, D, the second-rank H–H unit-vector reorientation correlation time as measured by NMR, τ_2, the Debye relaxation time, τ_D, and the static dielectric constant ϵ. These results are summarized in Table 4. For these quantities the TIP4P/FQ is perhaps in the best overall agreement with experiment, but the SPC/E model also performs very well. Note that the rotational correlation times for all models are somewhat too short. We also note that rotational times for other molecule-fixed unit vectors for different isotopic situations have also been measured

Table 4
Summary of previously calculated properties for the different water models for H_2O at 298 K

Model	D (10^{-9} m^2/s)	τ_2 (ps)	τ_D (ps)	ϵ
SPC/E	2.4 ± 0.4[a]	1.9 ± 0.1[a]	10 ± 3[a]	67 ± 10[a]
SPC/FQ	1.7 ± 0.1[b]	2.2 ± 0.1[b]	9 ± 3[b]	116 ± 18[b]
TIP4P	3.6 ± 0.2[c]	1.4 ± 0.2 [c]	7 ± 2[c]	53 ± 2[d]
TIP4P/FQ	1.9 ± 0.1[b]	2.1 ± 0.1[b]	8 ± 2[b]	79 ± 8[b]
TIP5P/E	2.8 ± 0.1[e]	1.55 ± 0.04[e]	–	92 ± 14[e]
Dang–Chang	2.1 ± 0.1[f]	–	–	–
Experiment	2.30[f]	2.5[g]	8.27 ± 0.02[h]	78[i]

[a] Ref. [82].
[b] Ref. [27].
[c] Ref. [83].
[d] Ref. [84].
[e] Ref. [61].
[f] Refs. [64,85].
[g] Refs. [17,61,82].
[h] Ref. [16].
[i] Ref. [86].

experimentally [18,78–81], but here we focus on results for neat H_2O.

The general conclusions, then, are that all of the simulation models give results for all of the spectroscopic observables that are qualitatively correct. Thus for the line shapes, theoretical peak shifts and widths are generally correct to within 10% or 20%, and for the ultrafast observables (echo peak shifts, dynamic line widths, nodal slopes, oscillation frequencies, and long-time decays) theoretical predictions are also correct to within say 50%. Given the great skill required to perform the ultrafast experiments, and the difficulties and ambiguities in calculating spectroscopic observables from classical simulation models, one can consider this level of agreement to be quite rewarding and satisfactory. In terms of choosing one model that best represents dynamics in liquid water, one can consider both the general agreement of a model with the dynamical properties listed in Table 4, and the general agreement of a model with both the short- and long-time properties measured by ultrafast vibrational spectroscopy. On this basis one might select the SPC/E model. This model also has the advantage of simplicity and computational ease and speed. Note, however, that for some of the longer-time dynamical properties, like the rotational correlation time, or the long-time decay of the FTCF (and hence of the echo peak shift and other ultrafast observables), which may well be of greatest importance with respect to water's role as a solvent, the SPC/E model appears to have dynamics that are too fast. The endorsement of the SPC/E model is also not meant to diminish the importance of polarizability, which is certainly expected to be essential when dealing with inhomogeneous systems (such as the liquid/vapor interface) or aqueous solutions.

Acknowledgments

J.L.S. is grateful for support from the National Science Foundation through Grant No. CHE-0446666, and from ACS in the form of a PRF-AC grant. J.R.S. is grateful to the Fannie and John Hertz Foundation for a graduate fellowship. M.D.F. and A.T. thank the AFOSR (F49620-01-1-0018) and DOE (DE-FG02-9ER14988) for support, respectively. We also thank Steven Rick and Tsun-Mei Chang for generously providing code for their water models, Rich Saykally for making available his experimental Raman spectra, Ben Auer for pointing out the errors in Ref. [26] mentioned herein, and Bruce Berne and Lars G.M. Pettersson for helpful discussions.

References

[1] P. Ball, Life's Matrix: A Biography of Water, Farrar, Straus, and Giroux, New York, 1999.
[2] J. McMurry, Organic Chemistry, Brooks/Cole Publishing Co., Pacific Grove, 1996.
[3] D. Voet, J.G. Voet, C.W. Pratt, Fundamentals of Biochemistry, John Wiley and Sons Inc., New York, 1999.
[4] A. Wallqvist, R.D. Mountain, Rev. Comput. Chem. 13 (1999) 183.
[5] B. Guillot, J. Mol. Liq. 101 (2002) 219.
[6] R.S. Fellers, C. Leforestier, L.B. Braly, M.G. Brown, R.J. Saykally, Science 284 (1999) 945.
[7] F.N. Keutsch, R.J. Saykally, Proc. Natl. Acad. Sci. USA 98 (2001) 10533.
[8] C.J. Burnham, S.S. Xantheas, J. Chem. Phys. 116 (2002) 5115.
[9] G.S. Fanourgakis, S.S. Xantheas, J. Phys. Chem. A 110 (2006) 4100.
[10] A.K. Soper, M.G. Phillips, Chem. Phys. 107 (1986) 47.
[11] A.K. Soper, Chem. Phys. 258 (2000) 121.
[12] A.H. Narten, H.A. Levy, J. Chem. Phys. 55 (1971) 2263.
[13] J.M. Sorenson, G. Hura, R.M. Glaeser, T. Head-Gordon, J. Chem. Phys. 113 (2000) 9149.
[14] Ph. Wernet, D. Nordlund, U. Bergmann, M. Cavalleri, M. Odelius, H. Ogasawara, L.Å. Näslund, T.K. Hirsch, L. Ojamäe, P. Glatzel, L.G.M. Pettersson, A. Nilsson, Science 304 (2004) 995.
[15] J.D. Smith, C.D. Cappa, K.R. Wilson, B.M. Messer, R.C. Cohen, R.J. Saykally, Science 306 (2004) 851.
[16] U. Kaatze, V. Uhlendorf, Z. Phys. Chem. 126 (1981) 151.
[17] J. Jonas, T. DeFries, D.J. Wilbur, J. Chem. Phys. 65 (1976) 582.
[18] J. Ropp, C. Lawrence, T.C. Farrar, J.L. Skinner, J. Am. Chem. Soc. 123 (2001) 8047.
[19] E. Harder, J.D. Eaves, A. Tokmakoff, B.J. Berne, Proc. Nat. Acad. Sci. 102 (2005) 11611.
[20] C.P. Lawrence, J.L. Skinner, J. Chem. Phys. 117 (2002) 8847.
[21] P.L. Silvestrelli, M. Bernasconi, M. Parrinello, Chem. Phys. Lett. 277 (1997) 478.
[22] H. Ahlborn, X. Ji, B. Space, P.B. Moore, J. Chem. Phys. 111 (1999) 10622.
[23] T. Hayashi, T. la Cour Jansen, W. Zhuang, S. Mukamel, J. Phys. Chem. A 109 (2005) 64.
[24] K. Hermansson, S. Knuts, J. Lindgren, J. Chem. Phys. 95 (1991) 7486.
[25] S.A. Corcelli, C.P. Lawrence, J.L. Skinner, J. Chem. Phys. 120 (2004) 8107.
[26] S.A. Corcelli, J.L. Skinner, J. Phys. Chem. A 109 (2005) 6154.
[27] S.W. Rick, S.J. Stuart, B.J. Berne, J. Chem. Phys. 101 (1994) 6141.
[28] J.R. Schmidt, S.A. Corcelli, J.L. Skinner, J. Chem. Phys. 121 (2004) 8887.
[29] S. Li, J.R. Schmidt, S.A. Corcelli, C.P. Lawrence, J.L. Skinner, J. Chem. Phys. 124 (2006) 204110.
[30] S. Li, J.R. Schmidt, A. Piryatinski, C.P. Lawrence, J.L. Skinner, J. Phys. Chem. B 110 (2006) 18933.
[31] K. Kwac, M. Cho, J. Chem. Phys. 119 (2003) 2247.
[32] K. Kwac, M. Cho, J. Chem. Phys. 119 (2003) 2256.

[33] J. Stenger, D. Madsen, P. Hamm, E.T.J. Nibbering, T. Elsaesser, Phys. Rev. Lett. 87 (2001) 027401.
[34] J. Stenger, D. Madsen, P. Hamm, E.T.J. Nibbering, T. Elsaesser, J. Phys. Chem. A 106 (2002) 2341.
[35] R. Laenen, C. Rauscher, A. Laubereau, Phys. Rev. Lett. 80 (1998) 2622.
[36] S. Woutersen, U. Emmerichs, H.-K. Nienhuys, H.J. Bakker, Phys. Rev. Lett. 81 (1998) 1106.
[37] S. Woutersen, H.J. Bakker, Phys. Rev. Lett. 83 (1999) 2077.
[38] G.M. Gale, G. Gallot, F. Hache, N. Lascoux, S. Bratos, J.-Cl. Leicknam, Phys. Rev. Lett. 82 (1999) 1068.
[39] J.C. Deàk, S.T. Rhea, L.K. Iwaki, D.D. Dlott, J. Phys. Chem. A 104 (2000) 4866.
[40] S. Yeremenko, M.S. Pshenichnikov, D.A. Wiersma, Chem. Phys. Lett. 369 (2003) 107.
[41] C.J. Fecko, J.D. Eaves, J.J. Loparo, A. Tokmakoff, P.L. Geissler, Science 301 (2003) 1698.
[42] C.J. Fecko, J.J. Loparo, S.T. Roberts, A. Tokmakoff, J. Chem. Phys. 122 (2005) 054506.
[43] J.B. Asbury, T. Steinel, C. Stromberg, S.A. Corcelli, C.P. Lawrence, J.L. Skinner, M.D. Fayer, J. Phys. Chem. A 108 (2004) 1107.
[44] T. Steinel, J.B. Asbury, S.A. Corcelli, C.P. Lawrence, J.L. Skinner, M.D. Fayer, Chem. Phys. Lett. 386 (2004) 295.
[45] J.B. Asbury, T. Steinel, K. Kwak, S.A. Corcelli, C.P. Lawrence, J.L. Skinner, M.D. Fayer, J. Chem. Phys. 121 (2004) 12431.
[46] J.J. Loparo, S.T. Roberts, A. Tokmakoff, J. Chem. Phys. 125 (2006) 194521.
[47] J.J. Loparo, S.T. Roberts, A. Tokmakoff, J. Chem. Phys. 125 (2006) 194522.
[48] S.T. Roberts, J.J. Loparo, A. Tokmakoff, J. Chem. Phys. 125 (2006) 084502.
[49] J.D. Eaves, A. Tokmakoff, P.L. Geissler, J. Phys. Chem. A 109 (2005) 9424.
[50] J.D. Eaves, J.J. Loparo, C.J. Fecko, S.T. Roberts, A. Tokmakoff, P.L. Geissler, Proc. Nat. Acad. Sci. 102 (2005) 13019.
[51] J.R. Schmidt, S.A. Corcelli, J.L. Skinner, J. Chem. Phys. 123 (2005) 044513.
[52] S. Mukamel, Principles of Nonlinear Optical Spectroscopy, Oxford, New York, 1995.
[53] R. Rey, K.B. Møller, J.T. Hynes, J. Phys. Chem. A 106 (2002) 11993.
[54] A. Piryatinski, C.P. Lawrence, J.L. Skinner, J. Chem. Phys. 118 (2003) 9664.
[55] A. Piryatinski, C.P. Lawrence, J.L. Skinner, J. Chem. Phys. 118 (2003) 9672.
[56] S.A. Corcelli, C.P. Lawrence, J.B. Asbury, T. Steinel, M.D. Fayer, J.L. Skinner, J. Chem. Phys. 121 (2004) 8897.
[57] K.B. Møller, R. Rey, J.T. Hynes, J. Phys. Chem. A 108 (2004) 1275.
[58] H.J.C. Berendsen, J.R. Grigera, T.P. Straatsma, J. Phys. Chem. 91 (1987) 6269.
[59] H.J.C. Berendsen, J.P.M. Postma, W.F. van Gunsteren, J. Hermans, in: B. Pullman (Ed.), Intermolecular Forces, Reidel, Dordrecht, 1981.
[60] W.L. Jorgensen, J. Chandrasekhar, J.D. Madura, R.W. Impey, M.L. Klein, J. Chem. Phys. 79 (1983) 926.
[61] S.W. Rick, J. Chem. Phys. 120 (2004) 6085.
[62] M.W. Mahoney, W.L. Jorgensen, J. Chem. Phys. 112 (2000) 8910.
[63] W.F. Murphy, J. Chem. Phys. 67 (1977) 5877.
[64] L.X. Dang, T.-M. Chang, J. Chem. Phys. 106 (1997) 8149.
[65] L.X. Dang, T.-M. Chang, A.Z. Panagiotopoulos, J. Chem. Phys. 117 (2002) 3522.
[66] D.A. McQuarrie, Statistical Mechanics, Harper and Row, New York, 1976.
[67] J.T. Fourkas, H. Kaswashima, K.A. Nelson, J. Chem. Phys. 103 (1995) 4393.
[68] P. Hamm, R.M. Hochstrasser, in: Ultrafast Infrared and Raman Spectroscopy, Markel Dekker, New York, 2001, p. 273.
[69] F. Franks (Ed.), Water: A Comprehensive Treatise, vol. 1, Plenum Press, New York, 1972.
[70] J.D. Smith, C.D. Cappa, K.R. Wilson, R.C. Cohen, P.L. Geissler, R.J. Saykally, Proc. Natl. Acad. Sci. USA 102 (2005) 14171.
[71] W.F. Murphy, H.J. Bernstein, J. Phys. Chem. 76 (1972) 1147.
[72] J.R. Scherer, M.K. Go, S. Kint, J. Phys. Chem. 78 (1974) 1304.
[73] C.P. Lawrence, J.L. Skinner, Chem. Phys. Lett. 369 (2003) 472.
[74] J.A. Poulsen, G. Nyman, P.J. Rossky, Proc. Natl. Acad. Sci. USA 102 (2005) 6709.
[75] R.A. Kuharski, P.J. Rossky, J. Chem. Phys. 82 (1885) 5164.
[76] H.A. Stern, B.J. Berne, J. Chem. Phys. 115 (2001) 7622.
[77] C.P. Lawrence, J.L. Skinner, J. Chem. Phys. 118 (2003) 264.
[78] Y.L.A. Rezus, H.J. Bakker, J. Chem. Phys. 123 (2005) 114502.
[79] Y.L.A. Rezus, H.J. Bakker, J. Chem. Phys. 125 (2006) 144512.
[80] H.-S. Tan, I.R. Piletic, M.D. Fayer, J. Chem. Phys. 122 (2005) 174501.
[81] I.R. Piletic, D.E. Moilanen, D.B. Spry, N.E. Levinger, M.D. Fayer, J. Phys. Chem. A 110 (2006) 4985.
[82] D.E. Smith, L.X. Dang, J. Chem. Phys. 100 (1994) 3757.
[83] K. Watanabe, M.L. Klein, Chem. Phys. 131 (1989) 157.
[84] M. Neumann, J. Chem. Phys. 85 (1986) 1567.
[85] K. Krynicki, C.D. Green, D.W. Sawyer, Faraday Discuss. Chem. Soc. 66 (1978) 199.
[86] A.D. Buckingham, Proc. R. Soc. London, Ser. A 238 (1956) 235.